



Comparative study for different demister locations in multistage flash (MSF) flash chamber (FC)

M. Khamis Mansour^{1,*}, Hassan E.S. Fath

Faculty of Engineering, Mechanical Department, Alexandria University, Alexandria, Egypt
Fax: +203 5971853; email: mdkhamis@gmail.com

Received 4 January 2013; Accepted 21 February 2013

ABSTRACT

Multistage flash (MSF) is a widely used technology in large capacity salted water desalination plants. The enhancement in the thermal performance of this technology is still prospective and promising. In this research, vapor flow through the flash chamber (FC) was studied. Flow development in 2D simulation model of a real FC was investigated. Trajectory of liquid droplets was calculated using Lagrange approach. The continuity and Navier–Stokes equations for the continuous phase “vapor” were solved simultaneously with the particle equation using two equations k – ϵ turbulence model. The computational model was verified by comparing the predicated results (vapor pressure drop through the FC demister and moist separation efficiency) with those obtained from the published experimental data. The comparison showed a good agreement between both results with maximum deviation of less than –19.16%, however, most of the disagreement between both results is fewer than 10%. Four different demister locations were addressed. The first three locations are: on the right, left, and middle side of the FC inlet gate while the fourth one is the demister splitting on both sides of the FC. A comparison between the four different FCs in MSF plant was conducted on a basis of targeting higher separation efficiency with a reasonable vapor pressure drop across the demister. Two different velocity profiles for the flashing vapor entering the demister were adopted for four different types of the FCs. It was found that the third FC design (FC-III) has a better performance in terms of higher separation efficiency with relatively lower vapor pressure drop. The study could be considered as benchmark and helpful guidelines in a design of the FC shape in MSF desalination plants.

Keywords: Separation efficiency; Wire mesh demister; Pressure drop; MSF desalination; Lagrange model; CFD

1. Introduction

In the multistage flash (MSF) process, vapor forms within the liquid bulk via flashing process and hot brine flow freely in series of successive flash chambers

(FCs), where flashing occurs because of the successive reduction of the stages’ pressure below the inlet brine temperature. Flashing process is one of the main features of the MSF in which scale formation on the surface of the tubes is eliminated. The flashed-off vapor condenses on the tubes of the preheater/

*Corresponding author.

¹Present address: Mechanical Department, Faculty of Engineering, Beirut Arab University, Riad El Solh 1150 20, Beirut, Lebanon. Tel. +961 71817351; Fax: +961 7 985060; email: m.mansour@bau.edu.lb

condenser units. Fig. 1 shows the overall configuration: one typical operating MSF chamber and its main components. Flashed brine in the form of vapor passes through demister and condenses on the condenser tubes. Distilled water is accumulated in a distillate tray and transferred to the next stage as shown in Fig. 1.

The demister is one of the main components inside the FC of the MSF plant, as it is responsible for achieving high quality of distilled water by retaining the salted liquid droplets entrained with the vapor flow to the condenser. Therefore, the demister should be featured by higher separation efficiency with lower pressure drop to satisfy the best thermal and hydraulic performance to the unit. The higher pressure drop and the higher loss in the temperature driving force between the stages occurred and hence the lower condensation temperature difference. On the other hand, the lower separation efficiency and the higher brine carryover thus cause scales on the condenser tubes harming the thermal performance of the condenser and shortening the life time of the condenser tubes. The wire mesh demister is the most widely used in MSF plants as a result of its features of low pressure drop, high separation efficiency, and reasonable capital cost. In this study, the wire mesh demister is used.

The literature review of the demister performance evaluation is classified into two categories. The first category focuses on empirical or semi-empirical correlation obtained for the separation/removal efficiency and the pressure drop across the demister. The second one is related to the numerical studies using computational fluid dynamics (CFD) modeling to simulate the demister performance. El-Dessouky et al. [1] presented an empirical model for pressure drop and the separation efficiency for the wire mesh demister pad. The correlation of the separation efficiency functions in vapor velocity, wire diameter, droplet size, and packing density. On the other hand, the wet pressure drop is affected by the packing density, wire diameter, and vapor velocity. Brunazzi and Paglianti [2] presented a

semi-empirical model for the demister design, which is built on previous analysis presented by Langmuir and Blodgett [3] and Pich [4], who evaluated the inertial capture efficiency for a single wire, expressed in terms of a dimensionless Stokes number. The analysis for industrial wire mesh packing is presented by Carpenter and Othmer [5] as a function of the demister pad thickness, the demister specific area, the stocks efficiency, and the number of mesh layers. A new model was presented by Brunazzi and Paglianti [6] for predicting the removal efficiency of complex wire mesh eliminators. This new model can be used for predicting separation efficiency of multilayer pads and composite separators.

A limited number of researches are found in the literature on demister separation efficiency using CFD technique. The CFD studies were done on two types of demisters: wave-plate (vane type) demisters and wire mesh demisters. Wang and Davies [7] used the commercial software Phoenics to carry out a comprehensive numerical investigation on the effect of inlet gas velocity, bend angle, rear pockets on separation efficiency, and pressure drop of wave-plate demister. They used Eulerian–Lagrangian approach in order to track the liquid droplets. The droplets have uniform diameters of 10, 15 and 20 μm . Standard $k-\varepsilon$ turbulence model was used to simulate the gaseous phase; turbulent dispersion effects on droplet trajectories were not taken into account. No comparison with experimental data was provided. Gillandt et al. [8] used the commercial software Fluent to simulate the flow in a zigzag classifier, comparing experimental and predicted data. The droplet size investigated was 0.1–1 mm. The authors pointed out that the use of low Re $k-\varepsilon$ turbulence model gives better results than the standard version of the model. Wang and James [9] investigated the separation efficiency of two wave-plate demisters by numerically simulating the flow field and droplet motion with comparison to experimental work of Phillips and Deakin [10]. They adopted Eulerian–Lagrangian approach to solve the trajectory of the liquid droplets coupling with the motion of the continued flow (flue gas) using flow data from Ansys CFX (commercial code). Standard $k-\varepsilon$ and low Re $k-\varepsilon$ turbulence models were used to solve the momentum equation of the continuous flow. Recently, Zhao et al. [11] conducted a numerical simulation of a wave-plate demister with various geometries and operating conditions in order to study the separation efficiency using FLUENT 6.1. They used Lagrange approach in order to track the liquid droplets. The results show that not only the vane spacing and flue gas velocity, but also vane height (including height of curve and upright region) and vane turning

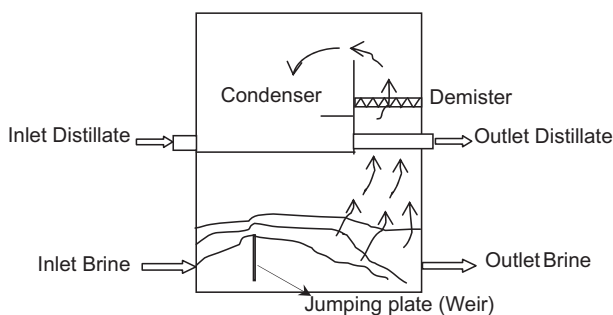


Fig. 1. MSF FC.

angles have a greater influence on the separation efficiency. There is no literature work on CFD modeling of the MSF wire mesh demisters except what was done by Rahimi and Abbaspour [12] and Al-Fulaij et al. [13]. Rahimi and Abbaspour [12] predicated pressure drop in a mist pad using numerical simulation via CFD. They validated their numerical result with those obtained from the available experimental data and empirical model of El-Dessouky et al. [1]. In regard to the calculation of the separation efficiency, a detailed model for tracking the liquid droplets through the vapor field was not given. It is not clear in their work how the demister and flow of vapor and brine droplets were modeled. The separation efficiency was calculated on a basis of introducing certain amount of liquid water with the vapor flow and calculating the accumulated water at the bottom of the chamber. More recently, Al-Fulaij et al. [13] presented numerical simulation model using CFD procedure. The demister simulation was represented by two different methods: porous media and tube bank. The porous media approach follows the Eulerian–Eulerian modeling method while two different models (Eulerian–Lagrangian and Eulerian–Eulerian) were adopted to simulate the demister as tube banks. In Eulerian–Eulerian (multiphase model), in either the porous media or tube bank approach, a constant sink value was set for the porous media and for the fluid region around the tubes in order to prevent brine droplet accumulation in the demister through simulations. However, the tube banks with discrete phase model approach follows the Eulerian–Lagrangian modeling method. In this model, the droplet particles escaped once they impact the demister surface in order to be eliminated from the calculation. The numerical results were validated against those obtained from the experimental work by El-Dessouky et al. [1]. In the three models, the inlet velocity of the mixture entered as uniform velocity. On the other hand, the injection of the liquid particles was done using uniform droplet diameters.

From the previous literature review, the following conclusions can be drawn:

- (1) There is a very limited number of the literature work on CFD modeling of the MSF wire mesh demisters.
- (2) The effect of entering vapor velocity profile to the FC on the demister performance has not been studied.
- (3) The injection of liquid droplets to the FC in the previous CFD works of modeling wire mesh demister had uniform diameters, in this study; the injected water droplets have different values along the FC width. This promotes the lift force to participate effectively with the inertia force (impaction) to formulate the demister separation efficiency.
- (4) The effect of the geometrical configuration of the FC on the performance of the wire mesh demister has not been addressed yet. The FC geometrical design contributes significantly to the behavior of the momentum change for the dispersed liquid droplets and the continuous vapor phase during flowing through the demister. Accordingly, it affects the demister pressure drop and separation efficiency. Therefore, in order to highlight this effect, four different FC configurations (FC-I, FC-II, FC-III, and FC-IV) are investigated in this study. Three of those FC designs are currently used in the industry; however, the third design (FC-III) is proposed as a novel FC design.

2. Mathematical modeling

The simulation of the saturated steam (water vapor) with water droplets was carried out through calculation of the governing equations for turbulent flow of continuous fluid “saturated steam” coupling with solving the governing equations of the discrete fluid “water droplets.” Physical properties of the continuous and dispersed fluid were taken as independent of temperature. Standard $k-\epsilon$ model was adopted as a turbulent model owing to its robustness and it has low computational time compared with the other turbulence model. On the other hand, Eulerian–Lagrangian approach was implemented to trace the water droplets’ motion and deposition. Assuming that the presence of droplets does not affect the continuous fluid flow (low concentration of droplets), the simulation of vapor droplets flow through the demister consists of the calculation of a single-phase turbulent flow and the subsequent calculation of droplet motion.

2.1. Model assumptions

The following assumptions which were adopted in this study are: (i) steady-state (ii) two dimensions flow, (iii) demister as porous media, (iv) incompressible Newtonian flow, (v) turbulent flow for vapor phase using $k-\epsilon$ model, (vi) isothermal flow so no heat/mass interaction between the gas phase and particles “inert exchange,” (vii) the diameter of the liquid droplets is varied along the FC width according to Rosin–Rammler diameter distribution relationship,

(viii) the liquid droplets have uniform shape as a sphere and they are stable during their movements, and (ix) the droplets are considered to be rebounded when they crash into any wall except the demister they are captured.

The continuous equation, Navier–Stokes equation and k – ε equation of continuous phase are described as:

2.2. Conservation of mass

$$\rho \left[\frac{\partial u}{\partial x} + \frac{\partial v}{\partial y} \right] = 0 \quad (1)$$

where ρ is the fluid density and u and v are fluid velocity components in x and y direction, respectively.

2.3. Conservation of momentum

It is derived from Newton's second law that states the rate of change of momentum equals the sum of forces acting on the fluid.

$$u \frac{\partial u}{\partial x} + v \frac{\partial u}{\partial y} = -\frac{1}{\rho} \frac{\partial P}{\partial x} + \nu \left[\frac{\partial^2 u}{\partial y^2} + \frac{\partial^2 v}{\partial x^2} \right] \quad (2)$$

$$u \frac{\partial v}{\partial x} + v \frac{\partial v}{\partial y} = -\frac{1}{\rho} \frac{\partial P}{\partial y} + \nu \left[\frac{\partial^2 v}{\partial x^2} + \frac{\partial^2 v}{\partial y^2} \right] \quad (3)$$

2.4. Transport equations for the standard k – ε model

The turbulence kinetic energy, k and its rate of dissipation, ε was obtained from the following transport equations:

$$\frac{\partial}{\partial x_j} (\rho k u_j) = \frac{\partial}{\partial x_j} \left[\left(\mu + \frac{\mu_t}{\sigma_k} \right) \frac{\partial k}{\partial x_j} \right] + \mu \frac{\partial u_i}{\partial x_j} \left[\frac{\partial u_i}{\partial x_j} + \frac{\partial u_j}{\partial x_i} \right] - \rho \varepsilon \quad (4)$$

$$\frac{\partial}{\partial x_j} (\rho \varepsilon u_k) = \frac{\partial}{\partial x_k} \left[\left(\mu + \frac{\mu_t}{\sigma_\varepsilon} \right) \frac{\partial \varepsilon}{\partial x_k} \right] + \frac{c_1 \varepsilon}{k} \mu \frac{\partial u_i}{\partial x_j} \left(\frac{\partial u_i}{\partial x_j} + \frac{\partial u_j}{\partial x_i} \right) - c_2 \rho \frac{\varepsilon^2}{k} \quad (5)$$

where μ_t is turbulent velocity and was calculated as in [14]: With $\mu_t=0.09$, $c_1=1.44$, $c_2=1.92$, $\sigma_k=1.0$, and $\sigma_\varepsilon=1.3$

In Eulerian–Lagrangian model, the continuum phase is fluid phase and it was treated by solving the

time-averaged Navier–Stokes equations, while the dispersed phase is solved by tracking a large number of particles, bubbles, or droplets through the calculated flow field. The dispersed phase can exchange momentum, mass, and energy with the fluid phase. A fundamental assumption made in this model is that the dispersed second phase occupies a low volume fraction, even though a high mass is acceptable. The particle or droplet trajectories are computed individually at specified intervals during the fluid phase calculation. In order to solve the equation of motion of the dispersed phase, it was assumed that:

- (1) Droplets are assumed as spheres.
- (2) There is no interaction between droplet–droplet.
- (3) No slip velocity between the droplets and the vapor.
- (4) The droplet–film interaction at the walls is negligible.
- (5) No liquid droplets breakup and no droplets re-entrainment.
- (6) The acting forces are the drag force and Saffman's lift force [15].

FLUENT predicts the trajectory of a discrete phase particle (droplet) by integrating the force balance on the particle, which is written in a Lagrangian reference frame. This force balance equates the particle inertia with the forces acting on the particle, and can be written (for the y direction in Cartesian coordinates) as:

$$\frac{du_p}{dt} = F_D(u - u_p) + F_y \quad (6)$$

where the first term represents the drag force, F_y is an additional acceleration (force/unit particle mass) term in the y direction which is Saffman's lift force in this study, and $F_D(u - u_p)$ is the drag force per unit particle mass and can be obtained from:

$$F_D = \frac{18\mu C_D Re}{\rho_p d_p^2} \quad (7)$$

where u is the vapor velocity, u_p the droplets velocity, μ the molecular viscosity of the vapor phase, ρ the vapor density, ρ_p is the density of the droplets, t is the relaxation time, and d_p is the droplets diameter. Re is the relative Reynolds number, which is defined as follows:

$$Re = \frac{\rho d_p |u_p - u|}{\mu} \quad (8)$$

The drag coefficient, C_D for smooth particles can be taken from

$$C_D = a_1 + \frac{a_2}{Re} + \frac{a_3}{Re^2} \tag{9}$$

where a_1 , a_2 , and a_3 are constants that apply over several ranges of Re given by [16].

2.5. Reference case—typical operating plant

The FC unit of Sidi Krir MSF (Alexandria—Egypt) [17] has been selected as the reference case study in this work for the FC dimensions. Sidi Krir MSF plant consists of 20 stages with a production capacity of 5,000 m³/day of desalinated water with brine recirculation flow rate of 1847 t/h. The plant first FC operating conditions are taken as the base case study. Fig. 2 shows the internal of Sidi Krir plant and FC internals' configuration. The typical first stage design conditions are: (a) brine inlet temperature is 110°C, (b) brine exit temperature is 106°C, (c) inlet brine mass flow rate is 1847 ton/hr, (d) stage pressure is 1.013 bars, (e) flashed vapor is 12.5 ton/hr for the full domain, (f) steam saturation temperature is 102°C. The simulation dimension and configuration of this unit is shown in Fig. 3.

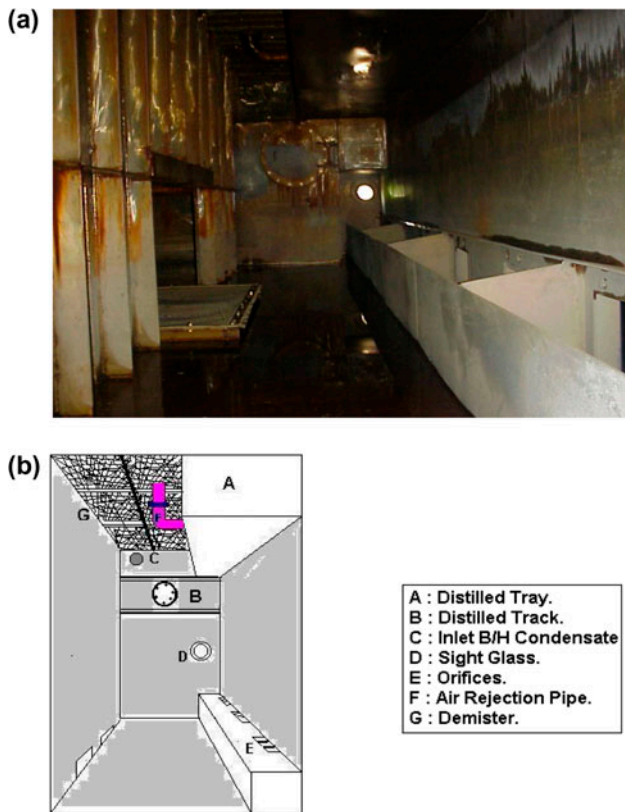


Fig. 2. Sidi Krir MSF plant & FC.

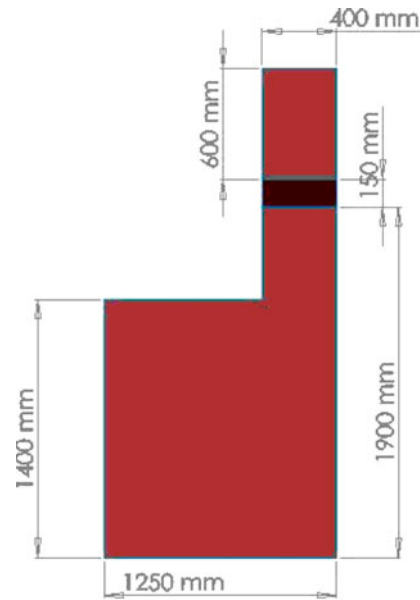


Fig. 3. The present design of FC “Sidi Krir”—FC-I.

2.6. Demister as porous media

Wire mesh mist eliminator, in the most general sense, is a simple porous blanket of metal or plastic wire that retains liquid droplets entrained by the vapor. As the vapor passed the mist eliminator, droplets impinged on the extensive surface of the wire, retained until they coalesce into large drops. When liquid drops reach sufficient size, they break away from the wire mesh and fall back against the rising vapor stream, El-Dessouky [1]. The performance of wire mesh eliminators depends on many design variables such as wire diameter, packing density, pad thickness, and material of construction. Table 1 shows the values of those physical parameters for the case study of this work.

In this study, the demister was treated as a porous medium that has a finite thickness over which the pressure change is defined as a combination of Darcy’s law and an additional inertial loss term:

$$\Delta P = - \left(\frac{\mu}{\alpha} + C_2 \frac{1}{2} \rho v^2 \right) \Delta m \tag{10}$$

Table 1
Specifications of the reference case’s demister

Height (m)	Wire diameter (mm)	Packing density (kg/m ³)	Surface area (m ² /m ³)	Porosity (%)
0.15	0.27	186.9	345	98

where μ is the laminar fluid viscosity, α is the permeability of the medium, C_2 is the pressure-jump coefficient, v is the velocity normal to the porous face, and Δm is the thickness of the medium. Appropriate values for α and can be C_2 calculated using the techniques described as follows:

$$\alpha = \frac{D^2}{150} \frac{\varepsilon^3}{(1-\varepsilon)^2} \quad C_2 = \frac{3.5}{D} \frac{(1-\varepsilon)}{\varepsilon^3} \quad (11)$$

where D is the mean mesh hole diameter and ε is the void fraction (porosity) defined as the volume of voids divided by the volume of the packed bed region.

2.7. Mesh generation and boundary conditions

Two meshes were generated for the calculations and the grid independence test. The coarse grid consisted of 21,900 cells with a maximum volume of 2.5×10^{-5} , and the fine grid consists of 350,400 cells with a maximum volume of 6.25×10^{-6} . The grids were generated by meshing all faces using regular quadrilateral mesh elements; the element size is 5 mm. The mesh geometry is presented in Fig. 4. Both solution-adaptive refinement and boundary-adaptive refinement were used in mesh adaptation facilities in ANSYS Fluent in the calculation with the coarse grid in order to get a reasonable solution. Due to the limit space, only the result of the grid independence test for FC-I case is presented in this work. Fig. 5 shows the difference in the local vapor velocity at the demister location for different mesh sizes for the present design. As shown in this figure, the curves are almost coincident after 87,600 as a number of cells.

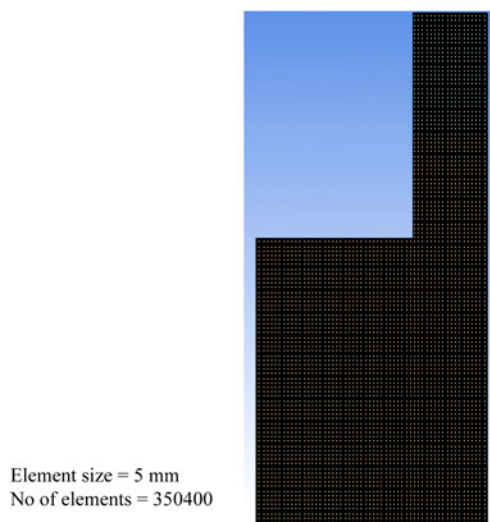


Fig. 4. Meshing domain of the present design of FC.

As the flow was wall dominated, the mesh extended into the viscous sublayer, such that $y^+ \sim 1$ to 5 in the wall bounded mesh points so that enhanced wall functions could be used with the $k-\varepsilon$ turbulent model. Eulerian–Lagrangian (discrete phase model) calculation method is employed to predict droplet transport and deposition. A second-order upwind scheme was applied for space discretization of the governing equations. The PRESTO and SIMPLE algorithms were adopted for the pressure interpolation and the velocity–pressure coupling, respectively. The turbulent stresses in the vapor momentum equation were modeled by the standard $k-\varepsilon$ model. The solution attains its convergence after several hundreds of iterations with residuals less than 10^{-4} for the continuity, turbulence parameters, and momentum equations.

The inlet condition of vapor flow is the velocity inlet. The entering velocity of liquid droplets was assumed to be equal to the inlet velocity of water vapor. In practice, the flow of the flashing vapor inside the FC is not uniform as expected, this is due to the flashing process which is not uniform [18]. Therefore, in order to simulate the behavior of the flashing process, a linear profile of the inlet velocity is proposed. Additionally, in order to enrich the performance comparison for the different FCs' configuration, a uniform velocity profile of the vapor flow is also proposed for both stages as shown in Fig. 6. The average velocity of the linear profile is equal to the value of the uniform velocity of 1.34 and 2.24 m/s for the high-temperature and low-temperature stage, respectively. The outlet

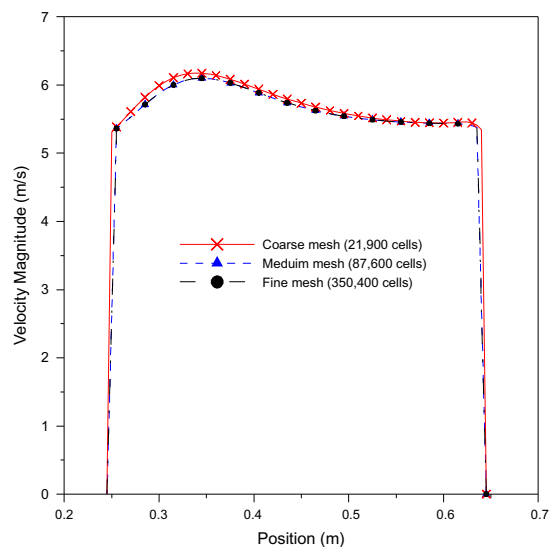


Fig. 5. Mesh independent.

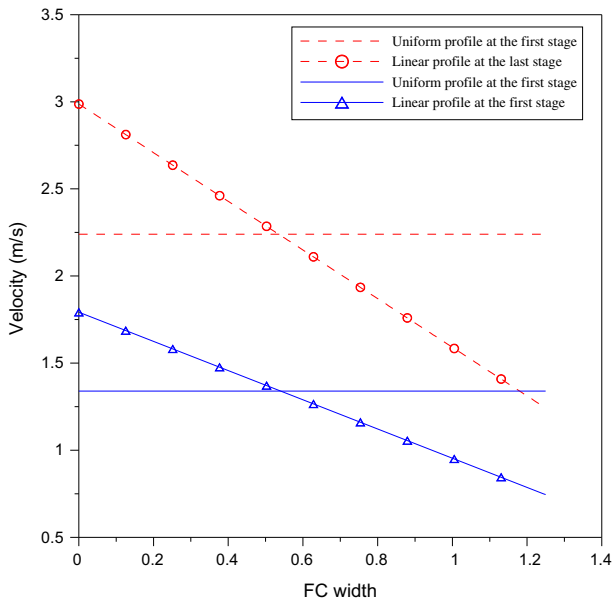


Fig. 6. Velocity profile along with the FC width.

condition is outflow as shown in Fig. 7. The particle size distribution of droplets is assumed to be in agreement with Rosin–Rammler diameter distribution. The maximum droplet size was taken as 1, 2, 3, 4 and 5 mm while the minimum as 1, 2, 3, 4 and 5 μm (corresponding to each maximum diameter, respectively),

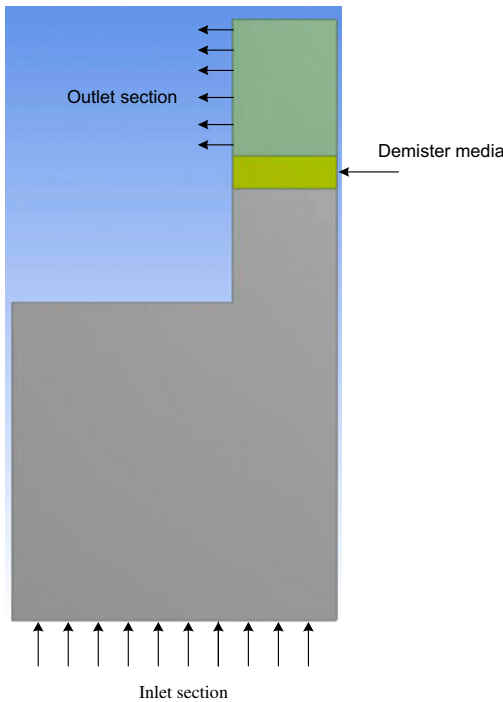


Fig. 7. Schematic diagram for boundary conditions.

and the spread parameter is 3.77. A number of 1,500 droplets were injected distributed along the FC inlet section for each droplet size. Also, uniform liquid droplets having mean diameter of 1, 2, 3, 4 and 5 mm were also investigated in order to compare the present study with the previous researches.

2.7. Model validation

The numerical calculations for the separation efficiency and demister wet pressure drop were compared with those calculated from El-Dessouky [1] empirical correlation. The comparison was studied by injection of three different sizes of the liquid droplets of 1, 3 and 5 mm. The entering vapor velocity was also taken as uniform distribution to the computational domain of a Plexiglas column of the experimental work of El-Dessouky [1]. A comparison of modeled and experimentally measured dependence of separation efficiency to vapor velocity is presented in Fig. 8. The results show that the simulated results agree well with the published experiments. The estimated uncertainties in the experimental work of El-Dessouky [1] were 4.6 and 3.2% from the true values for the pressure drop of the wet demister and separation efficiency, respectively. Fig. 9 shows that there is a good agreement between the theoretical results and calculated results of the empirical correlation with maximum deviation including the experimental uncertainty of less –19.16%, however, most of the disagreement between both results is under 10%. It was noticed that the computational model underpredicts most of the calculated separation efficiency as shown

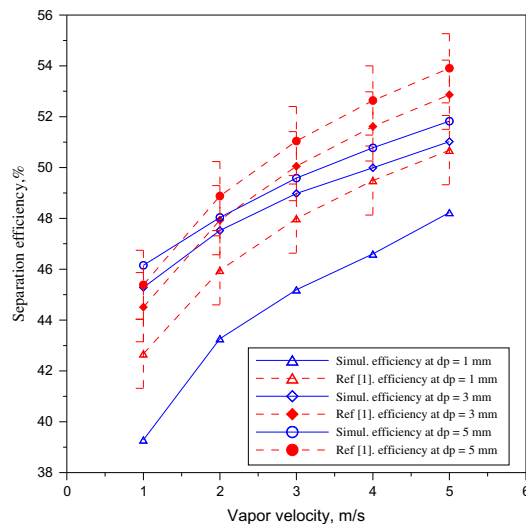


Fig. 8. Comparison of the published experimental and model calculated of separation efficiency at various vapor velocities.

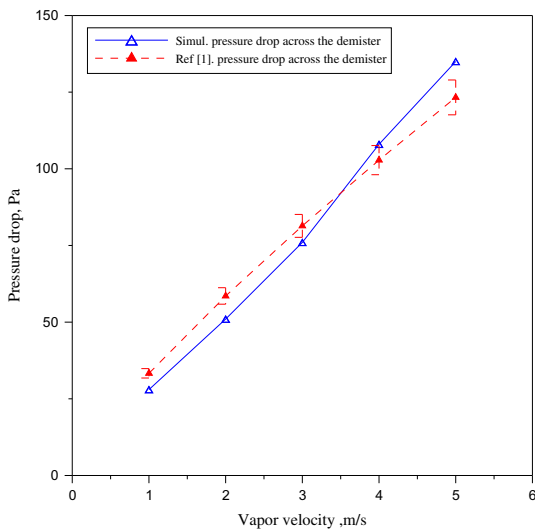


Fig. 9. Comparison of the published experimental and model calculated of demister pressure drop at various vapor velocities.

in Fig. 8. The reason is attributed to the assumptions which are adopted in the discrete phase model which causes the calculated results of the separation efficiency to be less than the experimental ones. In the numerical model, the interaction between the droplets themselves and the interaction between the droplets and the droplets-film at the walls were neglected.

3. Results and discussion

Efficiency of demister can be presented either as fractional removal or as fractional penetration. The summation of the removal and penetration efficiencies is equal to unity. Separation efficiency is a measure to the fraction of droplets in the vapor swept out by the wire mesh mist eliminator and is given by [1]:

$$\eta_{sp} = \frac{M_{in} - M_{out}}{M_{in}} \quad (12)$$

M_{in} and M_{out} are the masses of entrained water droplet by the vapor entering and leaving of the demister, respectively.

Four different demister locations of FC are studied and compared in terms of demister performance (separation efficiency and demister pressure drop). The configurations of the four chambers are displayed in Fig. 10. The first design (FC-I) is the reference case study (Sidi kiri plant—Egypt). The second design (FC-II), the demister is located at the left side of the FC, and in turn, the condenser chamber is placed at the right of the channel.

In the third design (FC-III), the demister is located at the middle of the chamber and the condenser chamber is splitted into two sections as shown in Fig. 10, and this configuration is proposed by the paper authors. The last design (FC-IV), the demister area is halved into two segments. The condenser chamber is accommodated in the middle of the FC.

In the following section, four design FCs will be assessed in terms of the velocity contours, pressure contours, pressure drop, and separation efficiency calculation. The input vapor velocity is assumed to enter as linear velocity profile for the high-temperature and low-temperature FC of the desalination plant. Due to the limited space of the paper, the velocity and pressure contours of the high-temperature stage will be displayed in the following Figures. As shown in Fig. 11, there is a harsh distribution of the velocity distribution at the demister channel for all different FCs configurations except for FC-III; the velocity contours are quite smooth at the demister entrance. The highest vapor velocity occurs in the second and last designs (FC-II and FC-IV) as a result of the highest entering velocity located at the left side of the FC at the direction of exit vapor channel for the second design FC-II. On the other hand, at the last design FC-IV, the smaller area of the exit channel renders an augmentation in the vapor velocity as shown in Fig. 11. This increase in vapor velocity causes an increase in the vapor pressure drop across the FC demister as shown in Fig. 12 and Table 2.

As shown in Table 2, the percentage increase in the demister pressure drop in the third design (FC-III) is around 13% over the pressure drop for the case study (FC-I) in both stages when the entering velocity is linear, while the percentage excesses in the demister pressure in the second and fourth design (FC-II and FC-IV) are 22% and 44%, respectively. On the other hand, when the entering velocity is uniform along the FC width, there is no difference between the four different FC designs in terms of the demister pressure drop.

Figs. 13 and 14 are prepared to illustrate the effect of FC configuration on the demister separation efficiency. One might expect that the FC which has the highest velocity magnitude at the demister channel would be featured by highest separation efficiency among the other FCs. This perception is not true, as seen from Fig. 13, the trend of separation efficiency of the third design (FC-III) takes place as the highest one although its vapor velocity magnitude at the demister channel is not the highest one. The explanation is, as it is known, the increase in vapor velocity augments the droplet momentum and hence, the separation efficiency is improved at expense of the effect of inertia

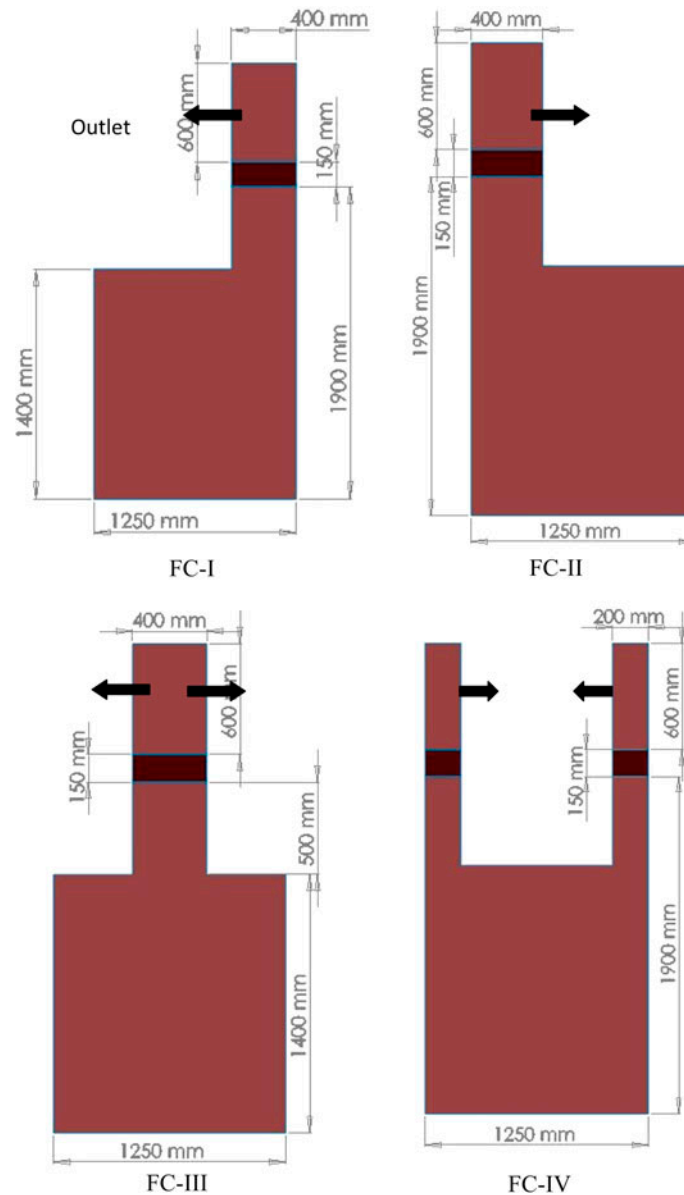


Fig. 10. Different configuration of FCs.

impaction. However, there is another factor that participates to formulate the separation efficiency which is the velocity variation along the demister width and the random size of the droplets. When the demister exposes to drastic variation in the vapor velocity, the nonuniform velocity distribution encourages the submicron droplets to escape easily from demister owing to the effect of droplet lift force. This force relies significantly on the small size of the droplets and mixture (vapor and brine droplets) direction and magnitude. For example, at maximum droplet diameter of 1 mm, the number of escaped droplets in the fourth design (FC-IV) is 1,323 while in the third

design (FC-III) is 577, for high-temperature stage. Accordingly, although FC-IV has the highest velocity magnitude at the demister area, it has the lowest separation efficiency trend owing to the effect of the lift force that dominates the effect of inertia impaction. Also, this explains why the demister performance of FC-I is higher than that of FC-II although the value of the velocity contours for the FC-II is higher than that of FC-I, as shown in Fig. 13.

It should be also noticed that the separation efficiency for all FCs at the high-temperature stage is lower than that of those FCs at low-temperature stage. The reason is attributed to the velocity variations at

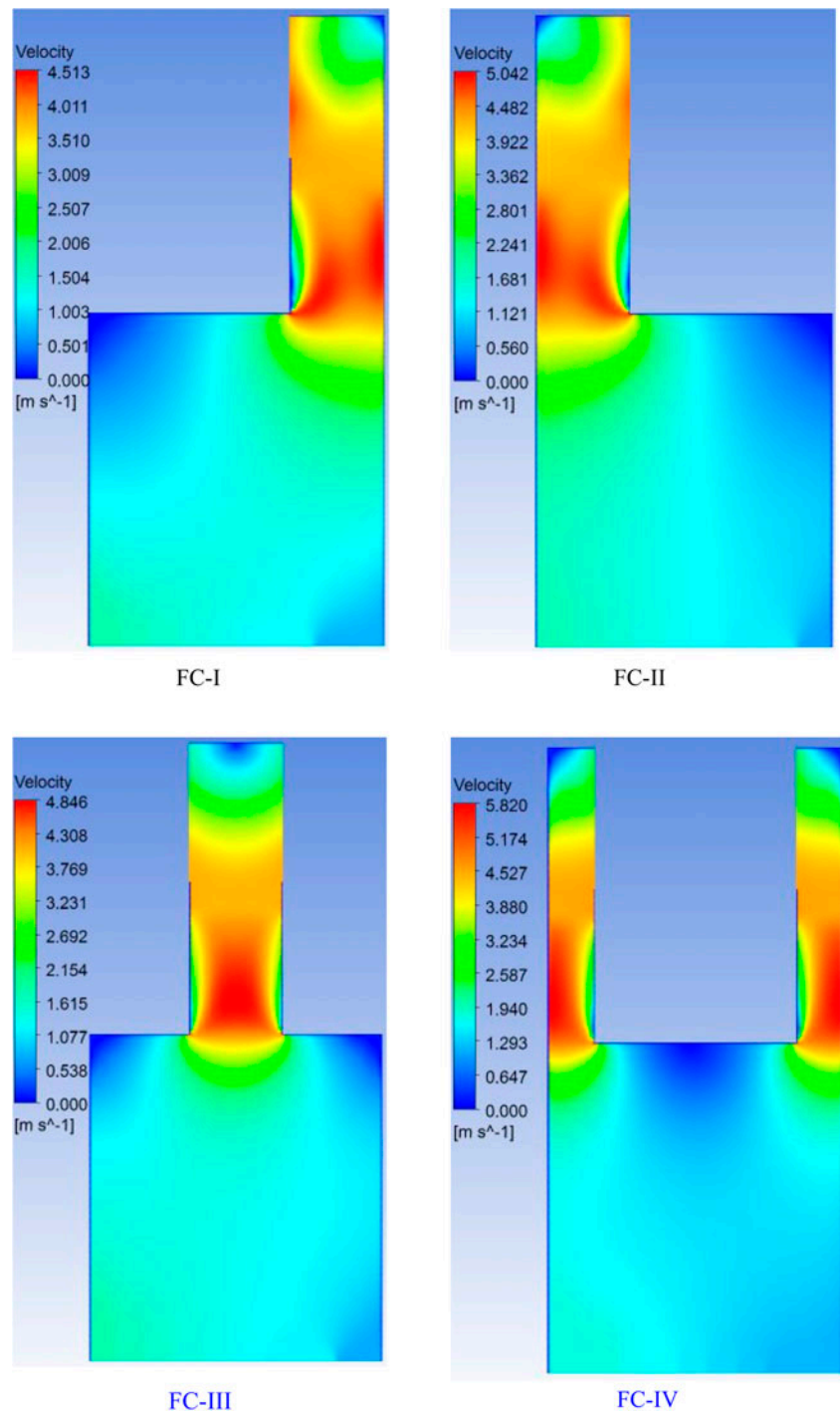


Fig. 11. Velocity contours for the first stage (linear velocity profile).

the demister zone in case of low-temperature stage which is higher than that of those in case of high-temperature stage. The turbulence intensity and eddies are augmented at higher velocity (at low-temperature stage). This encourages the effect of the lift force to participate significantly to control the value of the sep-

aration efficiency and hence the separation efficiency in the low-temperature stage is lower than that of the demister at high-temperature stage, and this conforms to what is experienced in industry. However, this is contradictory to what is expected and concluded from the previous studies. The previous studies [1,12,13]

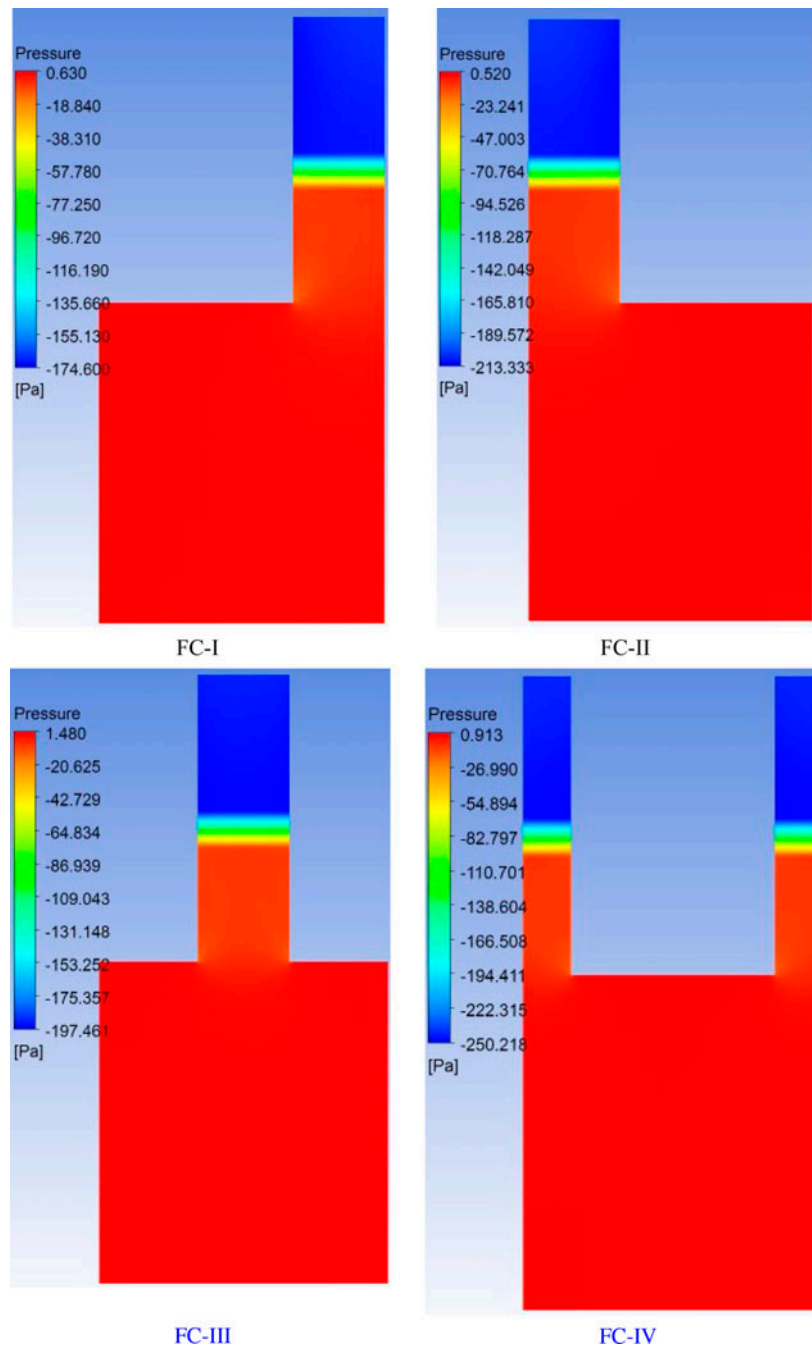


Fig. 12. Pressure contours for the 1st stage (linear velocity profile).

revealed that the increase in the vapor velocity usually accredits to an improvement in the separation efficiency provided that the increase in this velocity does not attain the flooding velocity value (above 5 m/s). Above this value would result in the increase of the re-entrainment rate of the brine droplets and subsequent increase in the product salinity [19]. The reason can be explained as follows. In the previous studies, the researchers addressed the demister sepa-

ration efficiency with injection of constant diameters of the liquid droplets of millimeter size while the lift force obviously appeared at the submicron droplets. In addition, the vapor velocity which enters the demister area was uniform. In order to compare with the previous studies, the effect of uniform vapor velocity profile with constant droplets diameter is presented in Fig. 14. It is interesting to see in Fig. 14 that the separation efficiency of the demister at the

Table 2
Comparison between the different FC configurations in terms of demister pressure drop

Case	FC-I (Pa)	FC-II (Pa)	FC-III (Pa)	FC-IV (Pa)
Linear velocity profile (high-temperature stage)	97	119	110	140
Linear velocity profile (low-temperature stage)	270	330	305	388
Uniform velocity profile (high-temperature stage)	118	118	117	117
Uniform velocity profile with of (low-temperature stage)	329	330	329	328.8

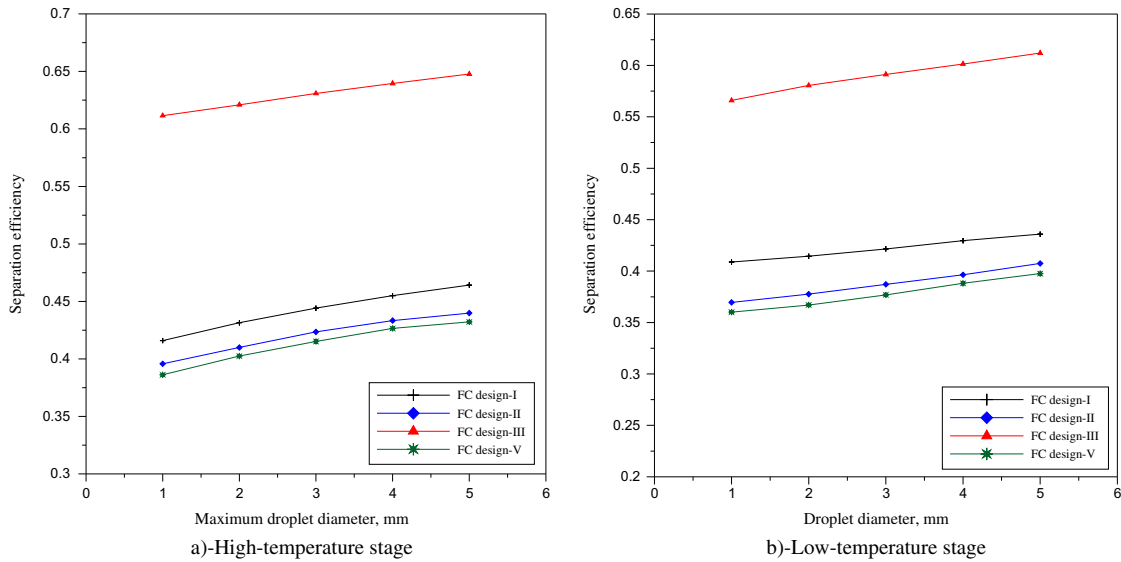


Fig. 13. Comparison between the different FC configurations in terms of separation efficiency at linear velocity profile with variable droplets diameter.

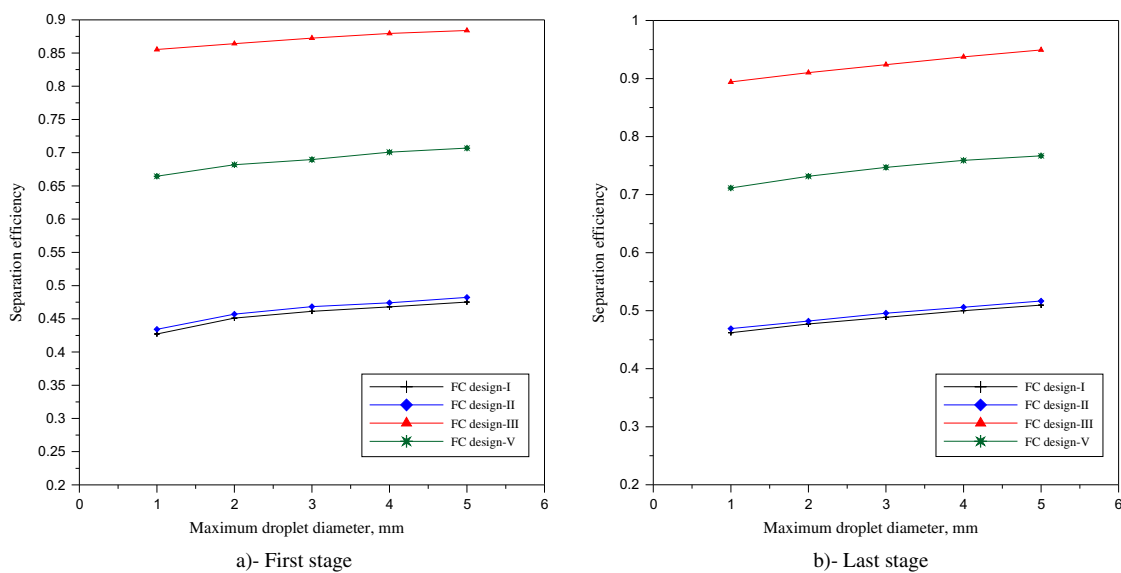


Fig. 14. Comparison between the different FC configurations in terms of separation efficiency at uniform velocity profile and uniform droplets diameter.

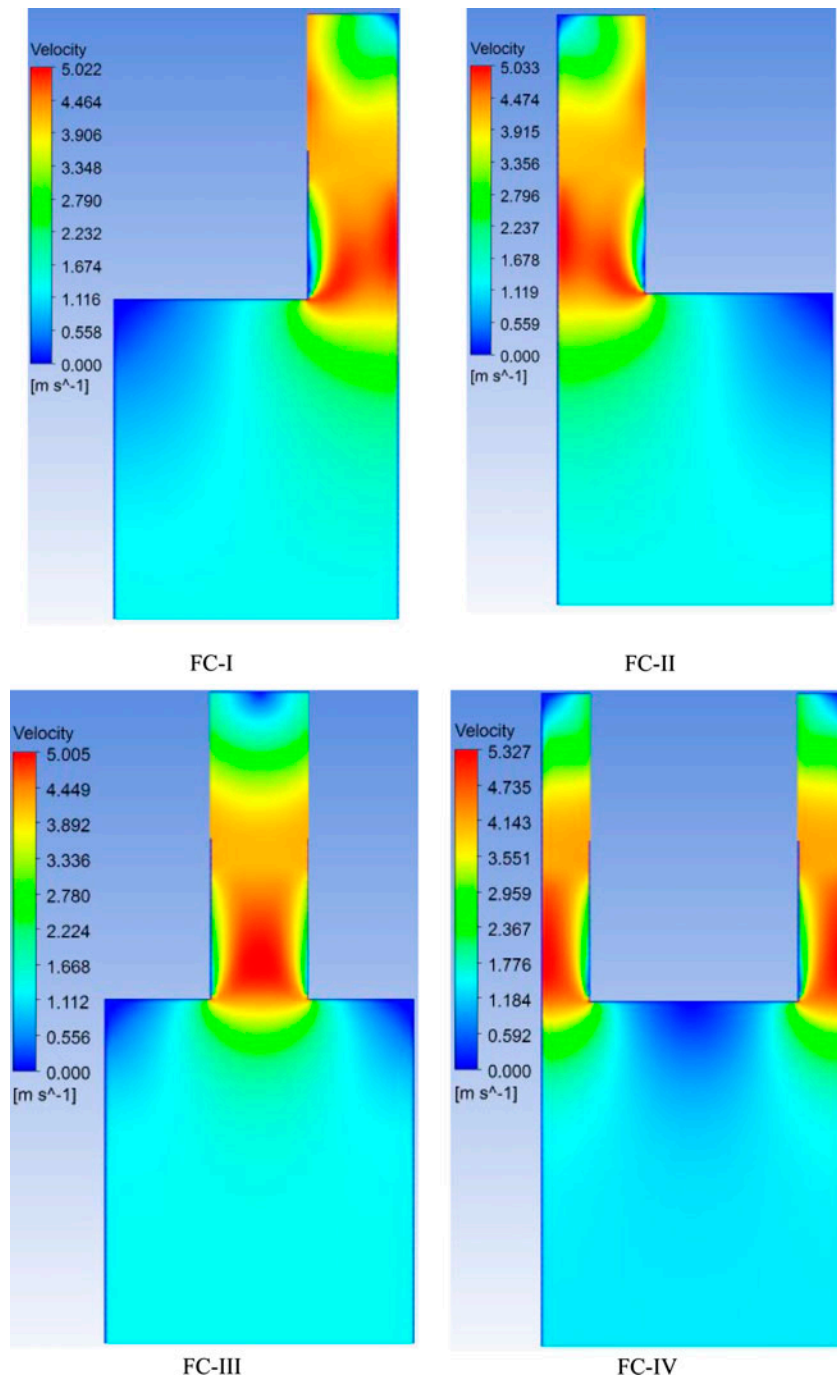


Fig. 15. Velocity contours for the first stage (uniform velocity profile).

low-temperature stage (at uniform velocity of 2.24 m/s) is higher than that of the demister at high-temperature stage (at uniform velocity of 1.34 m/s). In addition, the order of the demister performance of the four different FCs has been changed relatively. The third design FC-III still has the highest separation efficiency; however, the separation efficiency of the demister for the fourth design FC-IV is no longer the

lowest one as in Fig. 13. Additionally, the demister performance at the second FC design FC-II is slightly higher than that at FC-I. The explanation is related to the effect of the lift force attenuation at injection of uniform droplet diameters of millimeter size. Therefore, the competing effect between the inertia force and lift force is accredited to the effect of the inertia force only. Consequently, it is expected that the FC-IV

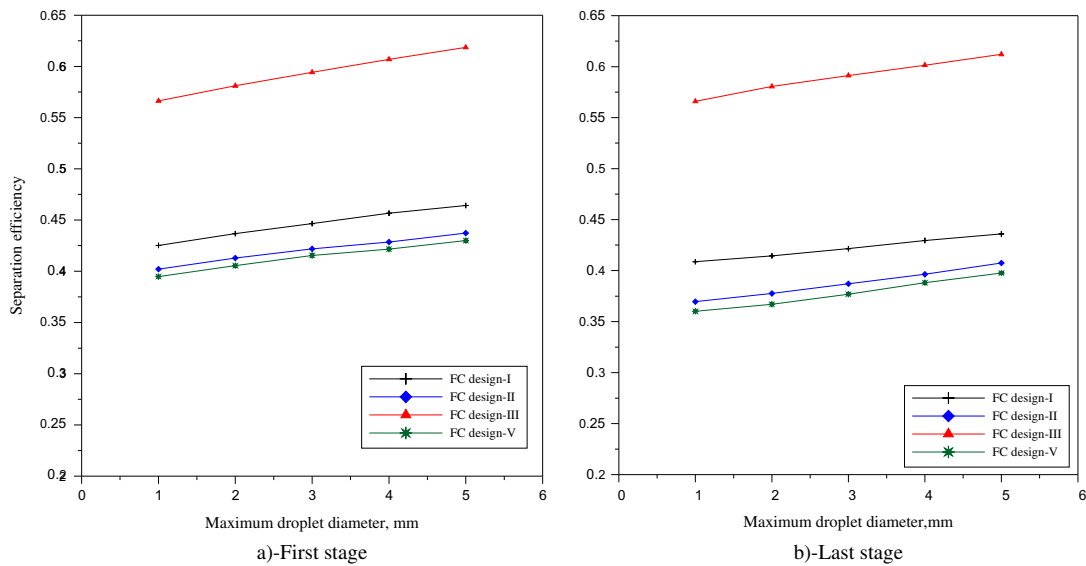


Fig. 16. Comparison between the different FC configurations in terms of separation efficiency at uniform velocity profile with variable droplets diameter (a) first stage and (b) last stage.

should have the highest demister performance in terms of the separation efficiency; however, as shown in Fig. 14, the FC-III has the highest one although it is expected that the magnitude of the velocity contours is smaller. The reason is the FC-III is featured by a quite uniform velocity distribution along the FC width with respect to that for FC-IV as shown in Fig. 15. Thus, the average vapor velocity at the demister zone for FC-III is higher than that for FC-IV and accordingly, the removal efficiency of the demister for FC-III is higher than that of the demister at FC-IV. As shown in Fig. 15, the magnitude of the vapor velocity for FC-II is insignificantly higher than that of FC-I, this explains why the demister performance for FC-II is slightly higher than that for FC-I.

The effect of entering uniform velocity with variable liquid droplets on the demister performance for the different FC configurations is illustrated in Fig. 16. The Figure shows that the FC-III still shows the highest demister performance and the FC-IV has the lowest one i.e. the effect of uniform vapor velocity profile on the different FCs design is similar to that of the linear vapor velocity profile. Also, the separation efficiency for the demister at the low-temperature stage is lower than that of the demister at the high-temperature stage.

4. Conclusion

Numerical study for the vapor flow inside the FC has been presented with a proposed new design for FC configuration. Trajectory of liquid droplets has been calculated using Eulerian–Lagrangian method.

The continuity and Navier–Stokes equations for the continuous phase “vapor” have been solved simultaneously with the particle equation. Four FC configurations were presented to study the effect of FC configuration of the demister thermal and hydraulic performance. In this study, the thermal performance is represented by the demister pressure drop which is translated to a drop in the steam saturation temperature. The hydraulic efficiency is represented by the separation efficiency. The following major conclusions can be drawn:

- (1) The first FC design (FC-I) has the lowest demister pressure drop in both stages (high- and low-temperature stages) when the vapor entering velocity has a linear profile. On the other hand, almost there is no difference between the different FC configurations for both stages and thus occurred when the entering vapor velocity has uniform value along the FC width.
- (2) The third FC design (FC-III) has the highest separation efficiency in both stages, the entering vapor velocity has linear or uniform profile. The center location of the demister at the third design FC-III enables the FC to have a better flow distribution through the demister channel. Accordingly, this enhancement in the flow distribution is translated to mitigation of the lift force influence and augmentation of the inertia impaction effect.
- (3) The third FC design (FC-III) has lower demister pressure drop than that of the other FC config-

urations except the FC-I. However, the percentage increase in the demister pressure drop for FC-III is almost 13% over that of demister for FC-I for both stages with linear velocity profile.

- (4) Although the fourth design FC-IV distributes the steam to the condenser chamber through the two sides, however, the demister of this FC design has the highest pressure drop and relatively low separation efficiency for both stages and the entering velocity profile is linear. This is attributed to the harsh velocity distribution at the demister zone. On the other hand, the FC-IV achieved the higher separation efficiency than that of FC-I and FC-II and this happened only when the liquid droplets had uniform diameters and hence the lift force is negated at this condition.
- (5) It was found that the thermal and hydraulic performances of the demister at the FC-I are higher than that of the demister at the FC-II for both stages when the entering vapor velocity is linear. However, the thermal and hydraulic performances of the demister at both chambers (FC-I and FC-II) are quiet similar when the profile of the entering vapor velocity is uniform and the droplets have uniform diameter.

The study could be considered as benchmark and helpful guidelines in a design of the FC shape in MSF desalination plants.

Nomenclature

d	— diameter, m
F_y	— additional acceleration (force/unit particle mass) term in x direction, m/s^2
g_x	— gravitational acceleration in x direction, m/s^2
M	— mass flow rate, kg/s
P	— pressure, Pa
u	— velocity in x direction, m/s
v	— velocity in y direction, m/s
x	— position x , m
y	— position y , m
t	— time, s

Greek letters

ρ	— density, kg/m^3
μ	— dynamic viscosity, Pa.s
α	— permeability of the medium, m
ε	— rate of turbulence dissipation or void fraction of demister (porosity)
η	— efficiency

Subscripts

i	— coordinate in i direction
j	— coordinate in j direction
p	— particle
sp	— separation efficiency

Acknowledgments

Computing infrastructure for this research was provided by grants from the Germany Egyptian Research Fund (GERF-STDF); the authors would like to acknowledge their support.

References

- [1] H. El-Dessouky, I. Alvtiiq, H. Ettouney, N. Al-Deffeeri, Performance of wire mesh mist eliminator, *Chem. Eng. Process.* 39 (2000) 129–139.
- [2] E. Brunazzi, A. Paglianti, Design of wire mesh mist eliminators, *Am. Inst. Chem. Eng. J.* 44 (1998) 505–512.
- [3] I. Langmuir, K.B. Blodgett, US army air forces technical, Report 5418, 1946.
- [4] J. Pich, Aerospace Science, C.N. Davies (Ed.), Academic Press, New York, NY, 1966 (Chapter 9).
- [5] C.L. Carpenter, D.F. Othmer, Entrainment removal by a wire-mesh separator, *Am. Inst. Chem. Eng. J.* 1 (1955) 549–557.
- [6] E. Brunazzi, A. Paglianti, Design of complex wire mesh-mist eliminators, *Am. Inst. Chem. Eng. J.* 4 (2000) 1131–1137.
- [7] Y. Wang, G.A. Davies, CFD Studies of separation of mists from gases using vane-type separators, *Chem. Eng. Res. Des.* 74 (1996) 232–238.
- [8] I. Gillandt, C. Riehle, U. Fritsching, Gas-particle flow in a comparison of measurements and simulations, *Forschung Im Ingenieurwesen—Eng. Res.* 62 (1996) 315–321.
- [9] Y. Wang, P.W. James, The Calculation of Wave-Plate Demister Efficiencies Using Numerical Simulation of the Flow Field and Droplet Motion, *Chem. Eng. Res. Des.* 76 (1998) 980–985.
- [10] H. Phillips, A.W. Deakin, Measurements of the collection efficiency of various demister devices, *Proceedings of the Fourth Annual Meeting of the Aerosol Society, Loughborough*, 1990.
- [11] J. Zhao, B. Jin, Z. Zhong, Study of the separation efficiency of a demister vane with response surface methodology, *J. Hazard. Mat.* 147 (2007) 363–369.
- [12] R. Rahimi, D. Abbaspour, Determination of pressure drop in wire mesh mist eliminator by CFD, *Chem. Eng. Process.* 47 (2008) 1504–1508.
- [13] H.F. Al-Fulaij, Dynamic Modeling of Multi Stage Flash (MSF) Desalination Plant. PhD-thesis (2011).
- [14] W. Tao, Numerical Heat Transfer, Xi'an Jiaotong University Publications, Xi'an, 207–211 1988.
- [15] P.G. Saffman, The lift on a small sphere in a slow shear flow, *J. Fluid Mech.* 22 (1965) 385–400.
- [16] H.P. Chen, Computational Fluid Dynamics, Water Conservancy and Hydroelectricity Publications, Beijing, pp. 97–103 1995.
- [17] H.E.S. Fath, The non-equilibrium factor and the flashing evaporation rate inside the flash chamber of a multi-stage flash desalination plant, *Desalination* 114 (1997) 277–287.
- [18] M. Khamis Mansour, H.E.S. Fath, Numerical simulation of flashing process in MSF flash chamber. *Desal. Water Treat.* (2012) 1–13, doi:10.1080/19443994.2012.734729.
- [19] H. Ettouney, Brine entrainment in multistage flash desalination, *Desalination* 182 (2005) 87–97.